Springer

Journal of Mechanical Science and Technology 23 (2009) 1476~1484

Journal of Mechanical Science and Technology

www.springerlink.com/content/1738-494x
DOI 10.1007/s12206-009-0351-2

Phase of acoustic impedance and performance of standing wave thermoacoustic coolers †

Insu Paek[1,*], Luc Mongeau[2], James E. Braun[3] and Shin You Kang[1]

[1]*Department of Mechatronics Engineering, Kangwon National University, Chuncheon, Gangwondo, 200-701, Korea*
[2]*Department of Mechanical Engineering, Mcgill University, Montreal, QC H3A 2K6, Canada*
[3]*Department of Mechanical Engineering, Purdue University, West Lafayette, IN 47907, USA*

(Manuscript Received October 27, 2008; Revised February 12, 2009; Accepted February 26, 2009)

Abstract

Investigations on the relations between the phase angle of the acoustic impedance at the driver piston and the system performance of a standing wave thermoacoustic cooler were performed. The system performance measured at a fixed acoustic power showed that the coefficient of performance of the standing wave thermoacoustic cooler increases as the phase angle increases when the stack temperature span is relatively low. The results were consistent with the simulation results obtained from DELTAE, a computer code based on linear thermoacoustic theory. Analysis on the temperature profiles along the stack showed that the cooling efficiency (COP) of the system could be decreased or increased as the phase angle of the acoustic impedance at the driver piston changes depending on the stack temperature spans.

Keywords: Coefficient of performance; Phase angle; Stack temperature span; Thermoacoustic cooler performance

1. Introduction

Electrodynamically driven standing wave thermoacoustic coolers use high amplitude sound waves generated from a driver to produce cooling energy [1]. The driver is properly tuned to maximize its acoustic power output at the frequency of interest by adjusting its stiffness, mass and piston area. The operating frequency is often chosen to match both mechanical resonance frequency of the driver and the acoustic resonance frequency of the pressure vessel. It enables to vanish both mechanical and acoustic reactances of the driver [2-5]. This leads to the maximum electroacoustic efficiency of the driver being achieved.

There is another way to achieve the maximum electroacoustic efficiency of the driver. In that case, the operating frequency of the driver is not the same as either the mechanical resonance frequency of the driver or the acoustic resonance frequency of the pressure vessel, but close to both. It is properly chosen to vanish the summation of the mechanical and acoustic reactances. Investigations on the system performances with off-resonance conditions are rare. One of the reasons why the off-resonance conditions are seldom used is that the advantage of doing that compared to the resonance conditions is not well known.

The objective of this paper was to investigate how the system efficiency is changed if the driver is operated off resonance. It was also to find the relationship between the phase angle of the acoustic impedance at the driver piston and the system efficiency, if any, in standing wave thermoacoustic coolers. To achieve the goal, both experimental investigations and computer simulations were performed. Discussions based on mathematical validations are also presented.

2. Experimental observations

Fig. 1 shows the schematic of the thermoacoustic cooler used in this study. It is a half wavelength

† This paper was recommended for publication in revised form by Associate Editor Yeon June Kang

*Corresponding author. Tel.: +82 33 250 6379, Fax.: +82 33 257 4190
E-mail address: paek@kangwon.ac.kr

standing wave thermoacoustic cooler having a moving magnet driver in one end and a hard wall in the other end. A 2.54 cm long rolled stack made of polyester films is sandwiched by two identical fin-end-tube aluminum heat exchangers. Key dimensions of the inside cross-section of the vessel are listed in Table 1.

Temperature, differential temperature, water flow rate, acoustic pressure, and acceleration signals were measured to evaluate the acoustic power and heat exchange rates. Within the water loop through the cold-side heat exchanger, a high-accuracy type T thermocouple probe (Thermoworks, HT-1) and a differential thermopile (Delta-T Company 75X) were installed to measure the temperature change of the water between inlet and outlet of each exchanger. The sensor uncertainties were 0.1 °C and 0.08 °C, respectively. The volume flow rate of water through the heat exchanger was measured with a precision axial paddle wheel turbine type flow meter (JLC International IR-Opflow). The uncertainty of the flow meter was 1 % of the measured value. The differential temperature of water across the heat exchanger was used to evaluate the heat delivery to the gas in the cold exchanger. A piezoelectric dynamic pressure sensor (PCB, 102A03) in a port near the piston was used to measure driver acoustic pressure. An accelerometer (PCB, 353B13) mounted on the carriage of the linear motor was used to measure piston acceleration. The input acoustic power was calculated based on accelerometer and driver pressure signals. More information of the experimental setup is available in the literature [5, 6].

Table 1. Key dimensions of the vessel, in millimeters.

Section	Upstream Diameter	Downstream Diameter	Length
Back Cavity	168	163	203
Driver Housing	89	114	184
Conical Enlargement	93	152	85
Hot Heat Exchanger	152	161	25
Stack	161	161	25
Cold Heat Exchanger	161	152	25
Conical Reduction	152	67	136
Resonator Tube	67	67	743

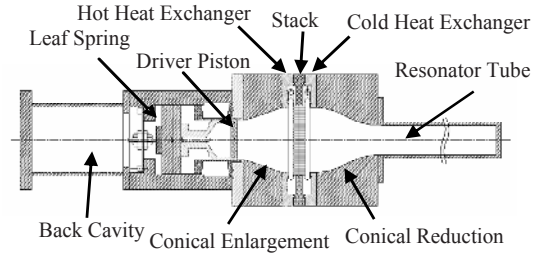

Fig. 1. Schematic of the standing wave thermoacoustic cooler. Dimensions of the parts are listed in Table 1.

The system performance is represented by the coefficient of performance (COP) [7], which is defined as

$$COP = \frac{\dot{Q}_c}{\dot{W}_{ac}}, \tag{1}$$

where $\dot{Q}_c$ is the cooling rate and $\dot{W}_{ac}$ is the acoustic power input. The COP was estimated with two different gas mixtures including 55 % helium – 45 % argon mixture and 45 % helium-56 % argon mixture at a fixed acoustic power input.

To check the accuracy of the experimental data, the relative uncertainty in the estimated cooling rates, was calculated. The heat transfer rate on the cold side was estimated by using [8]

$$\dot{Q} = \rho_w \dot{V}_w C_w \Delta T_w, \tag{2}$$

where, $\dot{Q}$ is the heat transfer rate, ρ_w is the density of water, $\dot{V}_w$ is the volume flow rate of water, C_w is the specific heat of water, and ΔT_w is the differential water temperature across the heat exchanger. Using the known uncertainties of the sensors for temperature, differential temperature, and volume flow rate, the relative uncertainty (or fractional uncertainty) of the heat transfer rate estimate was calculated from [9]

$$\delta_R \dot{Q} = \frac{\delta \dot{Q}}{\dot{Q}} = \sqrt{\left(\frac{\delta \dot{V}_w}{\dot{V}_w}\right)^2 + \left(\frac{\delta \rho_w}{\rho_w}\right)^2 + \left(\frac{\delta \Delta T_w}{\Delta T_w}\right)^2} \tag{3}$$

In Eq. (3), δ and δ_R denotes absolute and relative uncertainties, respectively. The contribution from the density is small compared to other terms; therefore, it was neglected.

Fig. 2 shows the measured COP with respect to the phase of the acoustic impedance at the driver. As shown in the figure, the COP increased as the phase angle increased. For the two different mixtures, the results were consistent. The measured data shown in

Table 2. Measured data obtained at a mean pressure of 0.69 MPa. Data are plotted in Fig. 2.

NO	He %	$\dot{W}_{ac}$ (W)	$\dot{Q}_c$ (W)	COP	Twi (K)	Tpilec (K)	$\delta_R \dot{Q}_c$ (%)
1	55	32.5	48.0	1.48	296.6	0.91	4.6
2	55	30.6	42.3	1.38	296.6	0.80	5.3
3	55	33.4	42.4	1.27	296.6	0.81	5.2
4	55	32.3	41.9	1.30	296.7	0.78	5.1
5	55	29.5	40.8	1.38	296.6	0.78	5.4
6	55	31.5	46.7	1.48	296.6	0.88	4.4
7	44	34.4	48.4	1.41	295.5	0.94	4.1
8	44	35.2	52.3	1.48	295.5	1.02	3.9
9	44	34.4	44.5	1.29	295.4	0.88	4.6

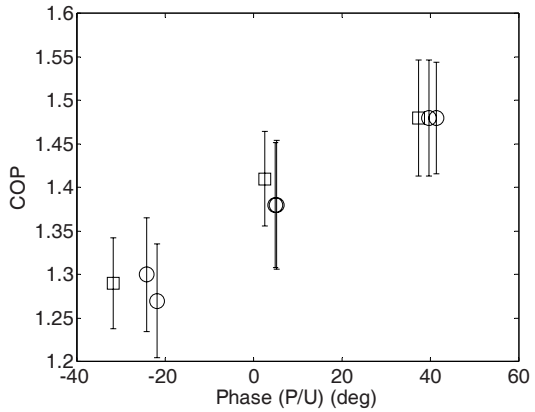

Fig. 2. Measured COP vs. Phase angle of acoustic impedance at the driver piston. □: 55% helium – 45% argon mixture, O: 44% helium – 56 % argon mixture. Data are plotted with error bars. Data are listed in Table 2.

Fig. 2 are listed in Table 2. The relative uncertainties of estimating the cold-side heat transfer rate were within 6 %.

3. Comparison with DELTAE

The system shown in Fig. 1 was modeled in a simulation program called DELTAE [10] based on linear thermoacoustic theory to compare the measured system performances with the predictions from the model. The unknowns and boundary conditions in DELTAE are defined as guess and target vectors, respectively [11]. The target vectors used include the stack end gas temperatures, phase angle between pressure and velocity at the driver, pressure and velocity amplitudes at the driver, and zero enthalpy flux condition at the termination end. The guess vectors

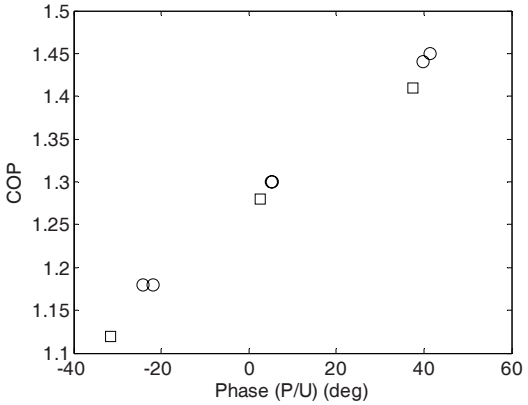

Fig. 3. COP vs. Phase angle of acoustic impedance at the driver piston from DELTAE simulations. □: 55% helium – 45% argon mixture, O: 44% helium – 56 % argon mixture.

were the mean pressure at the driver, amplitude and phase of the pressure at the driver, volume velocity amplitude at the driver, and heat transfer rates at both heat exchangers.

Fig. 3 shows the COP predicted from DELTAE with respect to the phase of the acoustic impedance at the driver piston. The results were consistent with the experimental observations.

4. Discussion

To know why the COP varies with the phase angle of the acoustic impedance at the driver, a mathematical analysis was performed.

4.1 The math

The COP of a thermoacoustic cooling system can be expressed as [11]

$$COP = \frac{-\dot{H}}{\dot{W}_{ac}} = -\left[(1-A) + \tan\phi \left(B + \frac{X}{\dot{W}_{ac}} \frac{dT_m}{dx} \right) \right] \qquad (4)$$

where $\dot{H}$ is the total power flowing along the stack which is negative for refrigerators, $\dot{W}_{ac}$ is the acoustic power input, ϕ is the phase angle between acoustic pressure and volume velocity, Z_{ac} is the acoustic impedance defined as the oscillating pressure, P, divided by the oscillating particle volume velocity, U, dT_m/dx is the slope of the temperature profile along the stack. A, B and X are defined as [11]

Table 3. Various Properties at the cold end of the stack for data sets in Fig. 4.

ϕ_{dr} (deg)	-31.7	2.6	37.4
1-A	0.3982	0.3948	0.3915
B	-0.4763	-0.4756	-0.4747
$\lvert Z_{ac}\rvert$ (Pa·s)	6.73E5	5.84E5	5.07E5
ϕ (º)	80.36	81.20	81.93
sin ϕ	0.986	0.988	0.990
tanϕ	5.887	6.460	7.058
dT_m/dx	-357.1	-303.0	-270.3

$$A = \mathbf{Re}\left[\frac{f_\kappa - \tilde{f}_\nu}{(1-\tilde{f}_\nu)(1+\varepsilon_s)}\right]\frac{T_m\beta}{(1+\sigma)}, \tag{5}$$

$$B = \mathbf{Im}\left[\frac{f_\kappa - \tilde{f}_\nu}{(1-\tilde{f}_\nu)(1+\varepsilon_s)}\right]\frac{T_m\beta}{(1+\sigma)}, \tag{6}$$

and

$$X = \frac{\rho_m c_p |U|^2}{2\omega A(1-\sigma)|1-f_\nu|^2}\mathbf{Im}\left[\tilde{f}_\nu + \frac{(f_\kappa - \tilde{f}_\nu)(1+\varepsilon_s f_\nu / f_\kappa)}{(1+\varepsilon_s)(1+\sigma)}\right] - \left(A_{fluid}K + A_{solid}K_{solid}\right) \tag{7}$$

In Eqs. (5)-(7) T_m is the mean temperature, σ is the Prandtl number, β is the thermal expansion coefficient, ρ_m is the density, c_p is the specific heat, ω is the angular frequency, A is the cross-sectional area, K is the thermal conductivity, the subscripts ν and κ represent viscous and thermal, respectively, f is the spatially averaged thermoviscous function, and ε_s is a correction for thermal properties of the solid wall [1].

At the cold-end of the stack, $(1-A)$ in Eq. (4) is always positive because the magnitude of A is known to be between 0 and 1 [12]. B should be always negative to yield a positive COP because both X and dT_m/dx are negative at the cold end [12]. Therefore, when the magnitude of dT_m/dx increases (steeper in slope), the COP decreases if other variables do not change much.

For the 44 % helium and 56 % argon data in Fig. 3, the stack temperature profiles were obtained from DELTAE and plotted in Fig 4.

When the phase angle of the acoustic impedance at the driver was -31.7, the magnitude of dT_m/dx at the cold end of the stack was large and as the phase angle increased, it decreased as shown in Fig. 4. This is consistent with the observation with Eq. (4). For the data points in Fig. 4, the variables in Eq. (4) were calculated and tabulated in Table 3.

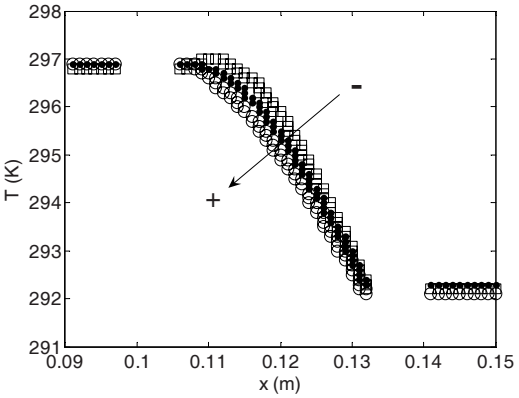

Fig. 4. Stack temperature profile vs. distance from driver piston with various phase angles of P/U at the driver. The direction of the arrow indicates increasing phase angles. O: +37.4°, •: 2.6° , □: -31.7°.

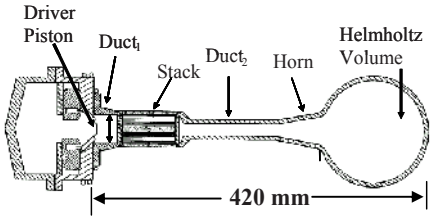

Fig. 5. Schematic of the standing wave thermoacoustic cooler (dimensions in millimeters).

4.2 Validation

More simulations were performed to fully understand this phenomenon over various operating conditions such as stack lengths and stack temperature spans. A standing wave thermoacoustic cooler with a quarter wavelength resonator [13] shown in Fig. 5 was used by varying stack lengths and stack end temperature differences. The mean pressure used was 1MPa and the working gas was helium. The acoustic power input at the driver piston was fixed to 10 W.

Fig. 6 shows the results with the stack length of 7.85 cm and four different stack temperature spans. The calculated properties obtained for the simulation are listed in Table 4. When the stack temperature span was 20 K and 40 K (Figs. 6(a) and 6(b)), the abnormal temperature profile along the stack (having a positive slope near the hot-side stack end) occurred. As the phase angle of the acoustic impedance at the driver piston increased, the abnormal temperature

profiles became more linear, and the COPs increased as shown in Table 4. This is consistent with the results obtained with the half wavelength standing wave thermoacoustic cooler used in this study.

When the stack temperature span was 60 K, the abnormal temperature profile did not occur, and as the phase angle increased from -40° to +40°, the temperature profile became slightly more linear although it did not change much. In this case, the COP did not change much as the phase angle increased. When the stack temperature span was 80K, the temperature profile changed slightly more nonlinear having larger magnitude of the temperature slope at the hot-side stack end than that at the cold-side stack end as the phase angle increased from -40° to +40°. In this case, the COP decreased as the phase angle increased.

The simulation result in Table 5 shows the relation between the cooling efficiency (COP) and the phase angle of the acoustic impedance at the driver for various stack lengths and stack temperature spans. For three different stack lengths, similar results with those in Fig. 6 were obtained. For each stack length, the COP increased with the phase angle when the stack temperature span was small, and it decreased with the phase angle when the stack temperature span was large. When the stack end temperature was in between, the COP did not change much with the phase angle. Fig. 7 shows the stack temperature profiles of simulation results presented in Table 4.

To find the relation between the phase angle and the stack temperature profile, Equation (4) can be rewritten for time harmonic waves as

$$\frac{dT_m}{dx} = \frac{\dot{H} - \dot{W}_{ac}((1-A) + B\tan\phi)}{X}, \tag{8}$$

where $\dot{W}_{ac}$ is the acoustic power.

In Eq. (8), X is always negative, and therefore dT_m/dx becomes positive when the numerator becomes negative. For a normal condition, $\left|\dot{W}_{ac}\left((1-A)+B\tan\phi\right)\right|$ is larger than $\left|\dot{H}\right|$ and the numerator becomes positive because both terms are

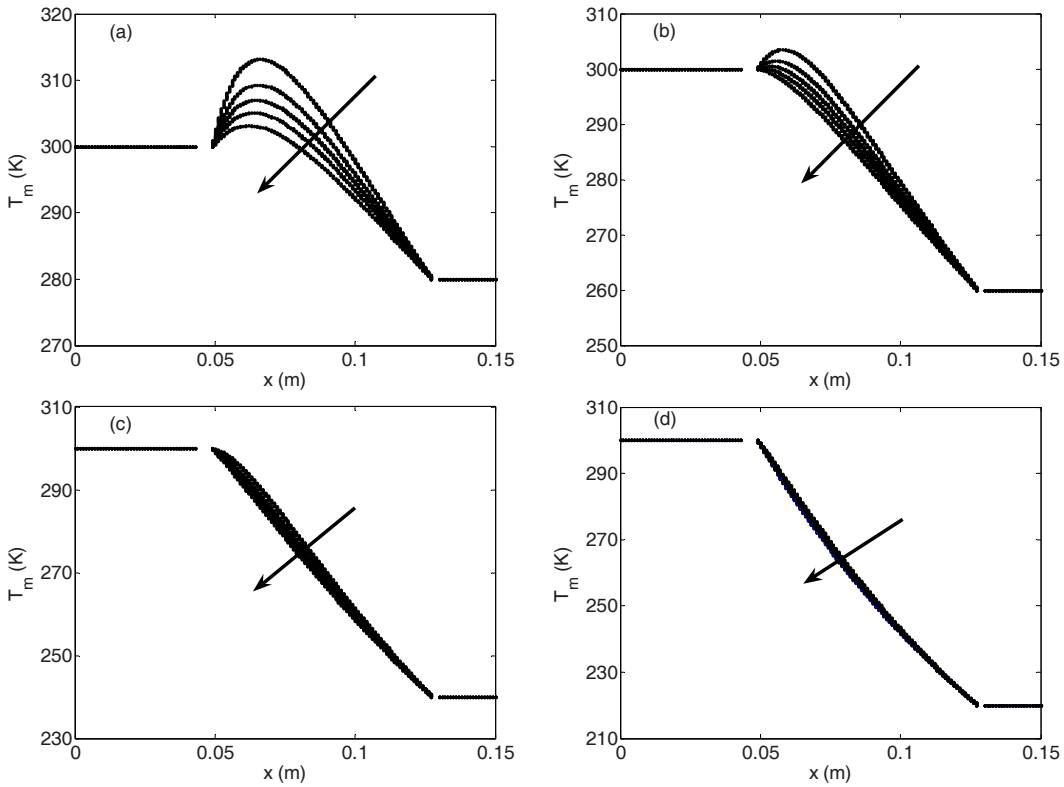

Fig. 6. Mean temperature (Tm) vs. distance (x) from driver piston for various stack end differential temperatures (Stack length: 7.85cm, (a):ΔT=20K, (b): ΔT=40K, (c): ΔT=60K, (d): ΔT=80K). The direction of the arrow indicates increasing the phase angle of P/U at the driver from -40° to +40° with an increment of 20°.

Table 4. Various properties at the hot and cold ends of the stack for data sets in Fig. 6. Stack length is 7.85cm.

ΔT (K)	Stack	ϕ_{dr} (°)	$\dot{H}$ (W)	1-A	B	tan ϕ	X	COP
20	Hot	-40	-8.63	0.8520	-0.3409	3.1474	-0.0033	0.86
		-20	-9.44	0.8476	-0.3452	3.5352	-0.0042	0.94
		0	-10.02	0.8441	-0.3485	3.8245	-0.0050	1.00
		20	-10.56	0.8405	-0.3518	4.1139	-0.0059	1.06
		40	-11.22	0.8356	-0.3562	4.5010	-0.0073	1.12
	Cold	-40	-8.63	0.8738	-0.3174	75.9828	-0.0200	0.86
		-20	-9.44	0.8701	-0.3215	65.8195	-0.0220	0.94
		0	-10.02	0.8672	-0.3247	67.0710	-0.0236	1.00
		20	-10.56	0.8641	-0.3280	69.2413	-0.0254	1.06
		40	-11.22	0.8600	-0.3323	72.4785	-0.0279	1.12
40	Hot	-40	-7.56	0.8446	-0.3480	3.6920	-0.0039	0.76
		-20	-8.05	0.8404	-0.3519	4.1335	-0.0049	0.80
		0	-8.36	0.8372	-0.3547	4.4354	-0.0057	0.84
		20	-8.62	0.8339	-0.3576	4.8066	-0.0067	0.86
		40	-8.87	0.8296	-0.3614	5.1994	-0.0081	0.89
	Cold	-40	-7.56	0.8880	-0.2999	69.4920	-0.0225	0.76
		-20	-8.05	0.8852	-0.3034	76.0919	-0.0247	0.80
		0	-8.36	0.8830	-0.3061	83.4405	-0.0265	0.84
		20	-8.62	0.8807	-0.3088	76.0741	-0.0284	0.86
		40	-8.87	0.8777	-0.3123	70.7882	-0.0310	0.89
60	Hot	-40	-6.08	0.8360	-0.3558	4.4378	-0.0047	0.61
		-20	-6.20	0.8322	-0.3592	4.9282	-0.0058	0.62
		0	-6.22	0.8293	-0.3616	5.2716	-0.0067	0.62
		20	-6.17	0.8264	-0.3641	5.6372	-0.0077	0.62
		40	-5.99	0.8226	-0.3672	6.1685	-0.0092	0.60
	Cold	-40	-6.08	0.9012	-0.2818	78.2152	-0.0258	0.61
		-20	-6.20	0.8991	-0.2847	74.1121	-0.0283	0.62
		0	-6.22	0.8975	-0.2869	84.9031	-0.0303	0.62
		20	-6.17	0.8959	-0.2890	80.5407	-0.0324	0.62
		40	-5.99	0.8938	-0.2917	81.0845	-0.0352	0.60
80	Hot	-40	-3.91	0.8261	-0.3644	5.5583	-0.0059	0.39
		-20	-3.59	0.8227	-0.3672	6.0637	-0.0072	0.36
		0	-3.26	0.8201	-0.3692	6.4376	-0.0082	0.33
		20	-2.85	0.8177	-0.3712	7.0569	-0.0093	0.29
		40	-2.20	0.8145	-0.3737	7.6135	-0.0109	0.22
	Cold	-40	-3.91	0.9133	-0.2634	87.1944	-0.0306	0.39
		-20	-3.59	0.9118	-0.2657	73.8230	-0.0372	0.36
		0	-3.26	0.9107	-0.2674	84.8648	-0.0357	0.33
		20	-2.85	0.9096	-0.2690	86.0638	-0.0381	0.29
		40	-2.20	0.9082	-0.2710	82.7722	-0.0414	0.22

negative. However, the numerator becomes negative when $\left|\dot{H}\right|$ is large. This means that the total power flowing through the stack is large, in other words, the cooling load applied to the cold side stack is large.

For a given length of stack, it seems that there exists a certain temperature gradient that would make a

Table 5. Cooling efficiency (COP) for various stack length and stack temperature spans.

Stack length (cm)	ΔT (K)	ϕ_{dr} (°)	*COP*
1.85	**5**	-40	2.80
		-20	2.87
		0	2.93
		20	2.99
		40	3.06
	20	-40	1.97
		-20	1.97
		0	1.98
		20	1.97
		40	1.97
	35	-40	0.72
		-20	0.64
		0	0.58
		20	0.51
		40	0.41
3.85	**10**	-40	1.69
		-20	1.77
		0	1.83
		20	1.89
		40	1.96
	40	-40	1.13
		-20	1.13
		0	1.13
		20	1.12
		40	1.10
	60	-40	0.48
		-20	0.41
		0	0.35
		20	0.28
		40	0.19
5.85	**20**	-40	1.14
		-20	1.21
		0	1.26
		20	1.31
		40	1.37
	40	-40	0.95
		-20	0.99
		0	1.01
		20	1.02
		40	1.03
	70	-40	0.50
		-20	0.46
		0	0.42
		20	0.38
		40	0.31

linear-like temperature profile across the stack. In that case, the COP is not much affected by the phase angle of acoustic impedance at the driver. The temperature span along the stack is determined by the cooling load applied to the cold side stack. As the cooling load gets smaller, the stack temperature profile becomes nonlinear. The magnitude of the slope at the hot-side stack end becomes larger than that at the cold-side stack. Nonlinear temperature profiles mean that there exist locations in the stack where the thermoacoustic heat pumping process from the hot-side to the cold side occurs inefficiently. Therefore, the COP gets lower than that of the case with a linear stack temperature profile. In that case, as the phase angle increases, the stack temperature profile becomes more nonlinear and the COP decreases. Also in that case, $\left|\dot{H}\right|$ is small regardless of tan ϕ, and dT_m/dx stays negative. This happens when the thermoacoustic cooler is mostly insulated and there is no heat load at the cold side of the stack.

However, as the cooling load increases, the temperature span decreases, and $\left|\dot{H}\right|$ becomes larger than $\left|\dot{W}_{ac}\left(\left(1-A\right)+B\tan\phi\right)\right|$. Such a small stack temperature span can be commonly encountered in reality when the stack is surrounded by highly effective heat exchangers with relatively large heat load. In that case, dT_m/dx partly becomes positive near the hot-side stack end and the stack temperature profile becomes nonlinear. The nonlinear temperature profile again makes the COP lower than that of the case with a linear stack temperature profile. This time, the COP is improved as the phase angle increases. It is because if the phase angle of oscillating pressure and particle velocity at the driver piston increases, it makes tan ϕ large in the stack, and finally makes the temperature profile more linear.

5. Conclusions

Investigations of the relation between the phase angle of the acoustic impedance at the driver piston and the COP were done both experimentally and by simulations using DELTAE. In experiments, it was observed that the COP increases with the phase angle of the acoustic impedance at the driver when the stack temperature span is relatively small compared with the stack length. The result obtained from DELTAE simulation was consistent with the experimental result when the heat load at the cold side stack was large. Analysis of the temperature profiles along the stack showed that when the stack temperature span was small for a given stack due to large heat load, the

stack temperature profile became nonlinear with a partial positive temperature gradient. Such nonlinear temperature profile became more linear and the COP increased as the phase angle of the acoustic impedance at the driver piston increased. When the stack temperature span was small for a given stack due to small heat load, the stack temperature profile became nonlinear but in the other direction than the large temperature case. This also decreased the COP as the phase angle increased.

Acknowledgment

The authors express their thanks to the Office of Naval Research (ONR), and the Air-Conditioning and Refrigeration Technology Institute (ARTI) for their financial support. The contribution of the Herrick Laboratories Technical staff is also gratefully acknowledged. Moreover, among the many who helped with this project, we are deeply indebted to Fred Keller of Carrier and Steve Memory of Modine for their help and support. This study was also supported by 2007 Research Grant from Kangwon National University.

List of symbols

A : Cross sectional area
A_{fluid} : Fluid area in stack
$Ar\%$: Percentage of argon in He-Ar mixture
A_{solid} : Solid area in stack
COP : Coefficient of performance
c_p : Specific heat
C_w : Specific heat of water
f_w : Spatially averaged thermo-viscous function
Im : Imaginary part
$He\%$: Percentage of helium in He-Ar mixture
$\dot{H}$: Total energy flux in watts
K : Thermal conductivity
P : Acoustic pressure
P_m : Mean pressure
$\dot{Q}$: Heat transfer rate
$\dot{Q}_c$: Cold-side heat transfer rate
Re : Real part
T_{pilec} : Differential temperature across cold-side heat exchanger
T_w : Temperature of water
T_{wi} : Temperature of water at the inlet of the cold-side heat exchanger
T_m : Mean temperature
U : Complex volume velocity
$\dot{V}_w$: Water volume flow rate
$\dot{W}_{ac}$: Acoustic power in watts
Z_{ac} : Acoustic impedance
β : Thermal expansion coefficient
γ : Specific heat ratio
Δ : Difference
δ : Uncertainty
$\delta_R\dot{Q}$: Relative uncertainty in heat transfer rate
ε_s : Correction for thermal properties of solid wall
ρ_w : Density of water
σ : Prandtl number
ω : Angular frequency
ϕ : Phase angle of Z_{ac} at a position
ϕ_{dr} : Phase angle of Z_{ac} at the driver piston in degrees

References

[1] G. W. Swift, *Thermoacoustics: A unifying perspective for some engines and refrigerators*, *Acoustical Society of America*, New York, USA, (2002).

[2] F. V. Hunt, *Electroacoustics: The Analysis of Transduction, and its Historical Background*, *Acoustical Society of America*, New York, USA, (1982). (Original work published by Wiley, New York, 1954).

[3] R. W. Wakeland, Use of electrodynamic drivers in thermoacoustic refrigerators, *J. Acoust. Soc. Am.* 107 (2000) 827-832.

[4] L. L. Beranek, *Acoustics*, *Acoustical Society of America*, New York, (1982). (Original work published by McGraw-Hill, New York, 1954).

[5] I. Paek, L. Mongeau, and J.E. Braun, A method for estimating the parameters of electrodynamic drivers in thermoacoustic coolers, *J. Acoust. Soc. Am.* 117 (2005) 185-193.

[6] I. Paek, J. E. Braun and L. Mongeau, Characterizing heat transfer coefficients for heat exchangers in standing wave thermoacoustic coolers, *J. Acoust. Soc. Am.* 118 (2005) 2271-2280.

[7] M. J. Moran and H. N. Shapiro, *Fundamentals of engineering thermodynamics*, *Wiley*, New York, USA, (2000).

[8] F. Incropera and D. Dewitt, *Fundamentals of heat and mass transfer*, *Wiley*, New York, USA, (1996).

[9] J. R. Taylor, *An introduction to error analysis*, *University Science Books*, California, USA, (1997), Eq. (3.47).

[10] W. C. Ward and G. W. Swift, *Design environment for low amplitude thermoacoustic engines (DeltaE)*, *J. Acoust. Soc. Am.* 95 (1994) 3671-3672. Software and user's guide available either from the US Los Alamos national laboratory thermoacoustics website at www.lanl.gov/thermoacoustics/ or from the Energy Science and Technology Software Center, US Department of Energy, Oak Ridge, Tennessee.

[11] W. C. Ward and G. W. Swift, *DELTAE Tutorial and User's Guide Version 5.1*, Los Alamos National Laboratory, New Mexico, USA, (2001).

[12] I. Paek, L. Mongeau and J.E. Braun, Performance Characterization of a Small-Capacity Thermoacoustic Cooler for Air-conditioning Applications, submitted in *J. Acoust. Soc. Am.*

[13] T. J. Hofler, *Thermoacoustic refrigerator design and performance*, *Ph.D. dissertation*, *Physics department*, *University of California San Diego*, California, USA, (1986).

Insu Paek received the B.S. degree in Mechatronics Engineering from Kangwon National University, Chuncheon, Korea, in 1997, the M.S. degree in Mechanical Engineering from the University of Texas at Austin, USA, in 2000, and the Ph. D. degree in Mechanical Engineering from Purdue University, West Lafayette, USA, in 2005. He worked as a postdoctoral researcher in Purdue University and McGill University in 2006 and 2007. He is currently a faculty member in the Department of Mechatronics Engineering, Kangwon National University, Chuncheon, Korea. His research interests include thermoacoustic cooling and power generation, solar heat driven absorption cooling., and wind power.

Luc Mongeau received the B.S. and M.S. degrees in mechanical engineering from the University of Montreal, QC, Canada, in 1984 and 1986, respectively, and the Ph. D. degree in Acoustics from Pennsylvania State University, University Park, USA, in 1990. He is currently a professor in the Department of Mechanical Engineering at McGill University, Montreal, QC, Canada. He has published over 50 archival journal publications on various topics related to acoustics and noise control. His research activities are in the flow and turbomachinery noise areas, as well as in the areas of voice production, and thermoacoustic refrigeration.

James E. Braun received the B.S. degree in Mechanical Engineering from the University of Massachusetts, USA, in 1976, and the M.S. and Ph. D. degrees in Mechanical Engineering from the University of Wisconsin, Madison, USA, in 1980 and 1988, respectively. He is currently a professor in the Department of Mechanical Engineering, Purdue University, West Lafayette, USA. Professor Braun's research combines the use of computer modeling, optimization, and experiments to study and improve the performance of thermal systems. He has published over 140 papers. Professor Braun is currently an associate editor for the international journal of HVAC&R Research.

Shin You Kang received the B.S. and M.S. degrees in the Department of Mechanical Design from Seoul National University, Seoul, Korea, in 1982, and 1986, respectively. He then received the Ph.D. in Mechanical Engineering at the same university in 1992. Professor Kang is currently a professor in the Department of Mechatronics Engineering, Kangwon National University, Chuncheon, Korea. His research interests include mechanical structure design, crash analysis, optimal design, computational structure analysis and evaluation.